JMM

A new fifth-order symmetrical WENO-Z scheme for solving Hamilton-Jacobi equations

Rooholah Abedian[*]

School of Engineering Science, College of Engineering, University of Tehran, Iran
Email(s): rabedian@ut.ac.ir

Abstract. This research describes a new fifth-order finite difference symmetrical WENO-Z scheme for solving Hamilton-Jacobi equations. This method employs the same six-point stencil as the original fifth-order WENO scheme (SIAM J. Sci. Comput. 21 (2000) 2126–2143) and a new WENO scheme recently proposed (Numer. Methods Partial Differential Eq. 33 (2017) 1095–1113), and could generate better results and create the same order of accuracy in smooth area without loss of accuracy at critical points simultaneously avoiding incorrect oscillations in the vicinity of the singularities. The new reconstruction is a convex combination of a fifth-order linear reconstruction and three third-order linear reconstructions. We prepare a detailed analysis of the approximation order of the designed WENO scheme. Some benchmark tests in 1D, 2D and 3D are performed to display the capability of the scheme.

1 Introduction

This research aims at obtaining numerical solutions for multi-dimensional Hamilton-Jacobi (HJ) equations of the form

$$\frac{\partial \phi}{\partial t}(\overrightarrow{x}, t) + H(\overrightarrow{x}, t, \phi, \nabla \phi) = 0, \quad \overrightarrow{x} = (x_1, \dots, x_d) \in \mathbb{R}^d. \tag{1}$$

The Hamiltonian, H, depends on $\nabla \phi$, ϕ and possibly on $\overrightarrow{x}$ and t. This type of equations are often appeared in many applications such as image processing, variational calculus, computer vision, material science and geometric optics [8, 11, 27, 41].

Although the solutions of HJ equations are usually continuous, their derivatives are discontinuous; even when the initial condition is smooth. Accordingly, it is better to study them in a suitable weak formulation. Such a weak formulation is presented by so-called *viscosity solutions* (see [13, 14, 26, 28,

42] and the references therein). Theoretically, the existence, uniqueness, and stability of the viscosity solution for (1) are proved by Crandall and Lions through appropriate assumptions on the Hamiltonian H and the initial condition $\phi(x,0) = \phi_0$. Computationally, monotone schemes [12, 15, 42] can be applied for approximation of these viscosity solutions. One of the weaknesses of monotone schemes is that they are first order accurate, thus they are too dissipative for most practical applications.

Since the HJ equations are well known to be closely related to conservation laws, hence successful numerical methods for them can be adjusted to approximate the solutions of the HJ equations [1–5]. Accordingly, in last decades, various schemes have been proposed for solving HJ equations (1). Among them that are proper to this research, the schemes of Osher and Sethian [30] and Osher and Shu [31] can be listed. These schemes are based on essentially non-oscillatory (ENO) schemes for approximating the solutions of hyperbolic conservation laws in [19, 39, 40]. Authors of [22] proposed a compact high-order method for solving the HJ equations. Their method is based on the weighted ENO (WENO) schemes for solving hyperbolic conservation laws proposed by Jiang and Shu in [23] and Liu et al. in [29]. Qiu and Shu [32–34] proposed another approach for solving these equations. Their schemes are based on original Hermite WENO reconstruction. Recently, Zheng and Qiu [46], Tao et al. [43], Zheng et al. [47] and Tao and Qiu [44] proposed other approaches based on Hermite WENO reconstruction for solving the HJ equations. ENO reconstruction with unstructured meshes for solving the HJ equations was proposed by Lafon and Osher in [25]. Abgrall [6], Zhang and Shu [45] used WENO reconstruction on triangular meshes for solving the HJ equations. In 2004, Serna and Qian applied Weighted power ENO reconstructions accompanying with upwind fluxes for HJ equations [37]. These scheme are based on power ENO schemes of [36] for solving conservation laws. Also, authors of [10] combined the Weighted power ENO reconstruction [37] and the mapped WENO reconstruction [20] and proposed a new method for solving HJ equations. In 2018, Ha et al. proposed a sixth-order finite difference WENO scheme based on exponential polynomials for HJ equations [18].

In general, WENO schemes for obtaining the solutions of the HJ equations have three steps: a monotone numerical Hamiltonian, a high-order WENO type reconstruction and an ordinary differential equations (ODE) solver. Osher and Shu in [31] performed a good and prefect discussion on monotone numerical Hamiltonians.

In literature, various ODE solvers have been introduced. The most popular ODE solvers are the strong-stability preserving Runge-Kutta (SSPRK) schemes [39, 40]. Later, Gottlieb et al. [16, 17] extended SSPRK schemes. Also, Shu [38] proposed a class of total variation diminishing (TVD) multi-step methods. Recently, a class of linear multi-step total variation bounded (TVB$_0$) schemes was proposed by Ruuth and Hundsdorfer [35]. These schemes need fewer CPU (central processing unit) time compared to SSPRK schemes. Another advantage of TVB$_0$ schemes compared to SSPRK or other multi-step methods is to avoid undershoots for great time steps. According to these aforementioned advantages, in this paper TVB$_0$ method of Ruuth and Hundsdorfer [35] is used.

The aim of this paper is to construct a high-order WENO type reconstruction. To construct a new method, the ideas of previous studies for hyperbolic conservation laws [7, 9, 21] will be used and extended. First, a six-point stencil will be chosen. Then, an optimum polynomial of fourth degree in a space of Legendre basis polynomials through this stencil is constructed. Now, four polynomials are required. Three of them are quadratic. It should be noted that these quadratic polynomials are based on four-point stencils, obtained from the six-point stencil. The last polynomial is achieved by simple algebraic calculations among the optimum function and the three functions previously computed. The role of the last function is only to recovery the accuracy in the smooth regions while in discontinuous

regions this polynomial is automatically removed by the procedure. Finally, similar to the procedure of WENO-Z scheme the non-linear weights are computed with the linear weights. Any symmetric selection of the constants, named the linear weights, will obtain the desired accuracy. Sum equals one is the only requirement for these symmetric constants.

This paper continuous as follows: the construction and implementation of new scheme for Hamilton-Jacobi equations will be described in Section 2. Section 3 demonstrates the accuracy and the resolution capability of the new scheme by several numerical examples. Concluding remarks are provided in Section 4.

2　Reconstruction of symmetrical WENO-Z scheme in Legendre basis

This section presents the framework of symmetrical WENO-Z scheme for solving the HJ equations briefly and afterwards develops the procedures of the new finite difference WENO method for both one and multi-dimensional HJ equations in detail.

2.1　Notations and preliminaries

First, consider the one-dimensional Hamilton-Jacobi equation with suitable boundary conditions,

$$\phi_t(x,t) + H(x,t,\phi,\phi_x) = 0, \qquad (x,t) \in \Omega \times (0,\infty), \tag{2}$$

$$\phi(x,t=0) = \phi_0(x). \tag{3}$$

For the sake of the simplicity, a uniform mesh with cells $I_x = [x - \Delta x, x]$ is supposed. Let $|I_x| = \Delta x$ to be the length of I_x. Also, the notations $\phi_j \equiv \phi_j(t) = \phi(x_j,t)$ and $\Delta^-\phi_j = \phi_j - \phi_{j-1}$ are considered. Consider the following semi-discrete method for Eq. (2)

$$\frac{d\phi_j(t)}{dt} = -\hat{H}(x_j,t,\phi_j,\phi_{x,j}^-,\phi_{x,j}^+) = F(\phi_j(t)), \tag{4}$$

where the term

$$\hat{H} := \hat{H}(x_j,t,\phi_j,\phi_{x,j}^-,\phi_{x,j}^+),$$

is the numerical flux function. The numerical flux is subject to the common conditions for numerical fluxes, such as Lipschitz continuity and consistency in the sense that $\hat{H}(x,t,\phi,\phi_x,\phi_x) = H(x,t,\phi,\phi_x)$. In this research the Lax-Friedrichs flux is used:

$$\hat{H}(x,t,\phi,u^-,u^+) = H(x,t,\phi,\frac{u^- + u^+}{2}) + \alpha\frac{u^- - u^+}{2}, \tag{5}$$

where $\alpha = \max_u |H_1(u)|$. Here H_1 is the partial derivative of H with respect to ϕ_x.

2.2　Reconstruction from point-values

Now, we would like to reconstruct the approximations of $\phi_{x,j}$ from the right and left sides of x_j. The remaining subsection describes by detailing the construction of the new finite difference WENO method

for solving HJ equations. The Legendre orthogonal monic polynomials, modified for the domain $[-1,0]$, are given by

$$L_0(x) = 1, \quad L_1(x) = x + \frac{1}{2}, \quad L_2(x) = x^2 + x + \frac{1}{6},$$
$$L_3(x) = x^3 + \frac{3}{2}x^2 + \frac{3}{5}x + \frac{1}{20}, \quad L_4(x) = x^4 + 2x^3 + \frac{9}{7}x^2 + \frac{2}{7}x + \frac{1}{70}.$$

S_1^-, S_2^- and S_3^- are used to denote the stencils $\{I_{x_{j-2}}, I_{x_{j-1}}, I_{x_j}\}$, $\{I_{x_{j-1}}, I_{x_j}, I_{x_{j+1}}\}$ and $\{I_{x_j}, I_{x_{j+1}}, I_{x_{j+2}}\}$, respectively. Also, S_1^+, S_2^+ and S_3^+ are used to denote the stencils $\{I_{x_{j-1}}, I_{x_j}, I_{x_{j+1}}\}$, $\{I_{x_j}, I_{x_{j+1}}, I_{x_{j+2}}\}$ and $\{I_{x_{j+1}}, I_{x_{j+2}}, I_{x_{j+3}}\}$, respectively. The notations $S^\pm$ are applied to denote the larger stencils $S_1^\pm \cup S_2^\pm \cup S_3^\pm$. Two polynomials of degree four, named optimal polynomials, are considered. These optimum polynomials, presented by $p_0^-(x) = \sum_{i=0}^4 a_i L_i(\frac{x-x_j}{\Delta x})^i$ on the left-biased stencil S^-, $p_0^+(x) = \sum_{i=0}^4 b_i L_i(\frac{x-x_j}{\Delta x})^i$, on the right-biased stencil S^+, are obtained to approximate $\phi_x(x_j, t)$ from left and right, respectively. Following [22, 48], $p_0^\pm(x)$ are uniquely generated by the equations

$$\int_{I_{x_{j+l}}} p_0^-(x)dx = \Delta^-\phi_{j+l}, \quad l = -2, \ldots, 2, \tag{6}$$

$$\int_{I_{x_{j+l}}} p_0^+(x)dx = \Delta^-\phi_{j+l}, \quad l = -1, \ldots, 3. \tag{7}$$

Now, by solving these linear systems the coefficients can be obtained explicitly to specify $p_0^\pm(x)$ and, later, the smoothness indicators can be computed

$$a_0 = \frac{\Delta^-\phi_j}{\Delta x},$$
$$a_1 = \frac{11\Delta^-\phi_{j-2} - 82\Delta^-\phi_{j-1} + 82\Delta^-\phi_{j+1} - 11\Delta^-\phi_{j+2}}{120\Delta x},$$
$$a_2 = \frac{-3\Delta^-\phi_{j-2} + 40\Delta^-\phi_{j-1} - 74\Delta^-\phi_j + 40\Delta^-\phi_{j+1} - 3\Delta^-\phi_{j+2}}{56\Delta x}, \tag{8}$$
$$a_3 = \frac{-\Delta^-\phi_{j-2} + 2\Delta^-\phi_{j-1} - 2\Delta^-\phi_{j+1} + \Delta^-\phi_{j+2}}{12\Delta x},$$
$$a_4 = \frac{\Delta^-\phi_{j-2} - 4\Delta^-\phi_{j-1} + 6\Delta^-\phi_j - 4\Delta^-\phi_{j+1} + \Delta^-\phi_{j+2}}{24\Delta x},$$

and

$$b_0 = \frac{\Delta^-\phi_j}{\Delta x},$$
$$b_1 = \frac{-27\Delta^-\phi_{j-1} - 110\Delta^-\phi_j + 192\Delta^-\phi_{j+1} - 66\Delta^-\phi_{j+2} + 11\Delta^-\phi_{j+3}}{120\Delta x},$$
$$b_2 = \frac{25\Delta^-\phi_{j-1} - 44\Delta^-\phi_j + 10\Delta^-\phi_{j+1} + 12\Delta^-\phi_{j+2} - 3\Delta^-\phi_{j+3}}{56\Delta x}, \tag{9}$$
$$b_3 = \frac{-3\Delta^-\phi_{j-1} + 10\Delta^-\phi_j - 12\Delta^-\phi_{j+1} + 6\Delta^-\phi_{j+2} - \Delta^-\phi_{j+3}}{12\Delta x},$$
$$b_4 = \frac{\Delta^-\phi_{j-1} - 4\Delta^-\phi_j + 6\Delta^-\phi_{j+1} - 4\Delta^-\phi_{j+2} + \Delta^-\phi_{j+3}}{24\Delta x}.$$

$p_1^-(x) = \sum_{i=0}^{2} \alpha_i L_i(\frac{x-x_j}{\Delta x})^i$ and $p_1^+(x) = \sum_{i=0}^{2} \tilde{\alpha}_i L_i(\frac{x-x_j}{\Delta x})^i$ are two quadratic functions defined on S_1^- and S_1^+, respectively. Following a similar discussion, the coefficients of these two polynomials can be obtained

$$\int_{I_{x_{j+l}}} p_1^-(x)dx = \Delta^- \phi_{j+l}, \quad l = -2, -1, 0, \tag{10}$$

$$\int_{I_{x_{j+l}}} p_1^+(x)dx = \Delta^- \phi_{j+l}, \quad l = -1, 0, 1, \tag{11}$$

$p_2^-(x) = \sum_{i=0}^{2} \beta_i L_i(\frac{x-x_j}{\Delta x})^i$ and $p_2^+(x) = \sum_{i=0}^{2} \tilde{\beta}_i L_i(\frac{x-x_j}{\Delta x})^i$ are two second degree polynomials defined on S_2^- and S_2^+, respectively. Following the above procedure, the coefficients of both function can be acquired

$$\int_{I_{x_{j+l}}} p_2^-(x)dx = \Delta^- \phi_{j+l}, \quad l = -1, 0, 1, \tag{12}$$

$$\int_{I_{x_{j+l}}} p_2^+(x)dx = \Delta^- \phi_{j+l}, \quad l = 0, 1, 2, \tag{13}$$

$p_3^-(x) = \sum_{i=0}^{2} \gamma_i L_i(\frac{x-x_j}{\Delta x})^i$ and $p_3^+(x) = \sum_{i=0}^{2} \tilde{\gamma}_i L_i(\frac{x-x_j}{\Delta x})^i$ are two quadratic functions defined on S_3^- and S_3^+, respectively. Following the above procedure, the coefficients of these functions can be calculated

$$\int_{I_{x_{j+l}}} p_3^-(x)dx = \Delta^- \phi_{j+l}, \quad l = 0, 1, 2, \tag{14}$$

$$\int_{I_{x_{j+l}}} p_3^+(x)dx = \Delta^- \phi_{j+l}, \quad l = 1, 2, 3, \tag{15}$$

where

$$
\begin{aligned}
&\alpha_0 = \frac{\Delta^- \phi_j}{\Delta x}, && \tilde{\alpha}_0 = \beta_0 = \frac{\Delta^- \phi_j}{\Delta x}, \\
&\alpha_1 = \frac{\Delta^- \phi_{j-2} - 4\Delta^- \phi_{j-1} + 3\Delta^- \phi_j}{2\Delta x}, && \tilde{\alpha}_1 = \beta_1 = \frac{-\Delta^- \phi_{j-1} + \Delta^- \phi_{j+1}}{2\Delta x}, \\
&\alpha_2 = \frac{\Delta^- \phi_{j-2} - 2\Delta^- \phi_{j-1} + \Delta^- \phi_j}{2\Delta x}, && \tilde{\alpha}_2 = \beta_2 = \frac{\Delta^- \phi_{j-1} - 2\Delta^- \phi_j + \Delta^- \phi_{j+1}}{2\Delta x}, \\
&\tilde{\beta}_0 = \gamma_0 = \frac{\Delta^- \phi_j}{\Delta x}, && \tilde{\gamma}_0 = \frac{3\Delta^- \phi_{j+1} - 3\Delta^- \phi_{j+2} + \Delta^- \phi_{j+3}}{\Delta x}, \\
&\tilde{\beta}_1 = \gamma_1 = \frac{-3\Delta^- \phi_j + 4\Delta^- \phi_{j+1} - \Delta^- \phi_{j+2}}{2\Delta x}, && \tilde{\gamma}_1 = \frac{-5\Delta^- \phi_{j+1} + 8\Delta^- \phi_{j+2} - 3\Delta^- \phi_{j+3}}{2\Delta x}, \\
&\tilde{\beta}_2 = \gamma_2 = \frac{\Delta^- \phi_j - 2\Delta^- \phi_{j+1} + \Delta^- \phi_{j+2}}{2\Delta x}, && \tilde{\gamma}_2 = \frac{\Delta^- \phi_{j+1} - 2\Delta^- \phi_{j+2} + \Delta^- \phi_{j+3}}{2\Delta x}.
\end{aligned}
\tag{16}
$$

The new symmetrical WENO-Z reconstruction on cells $I_{x_j} = [x_{j-1}, x_j]$ and $I_{x_{j+1}} = [x_j, x_{j+1}]$ is considered as follow

$$R^{\pm}(x) = \frac{w_0^{\pm}}{d_0} \left[p_0^{\pm}(x) - d_1 p_1^{\pm}(x) - d_2 p_2^{\pm}(x) - d_3 p_3^{\pm}(x) \right] + w_1^{\pm} p_1^{\pm}(x) + w_2^{\pm} p_2^{\pm}(x) + w_3^{\pm} p_3^{\pm}(x). \tag{17}$$

Here, $p_m^{\pm}(x)$, $m = 1, 2, 3$, determined by Eqs. (10)-(15), are the third-order reconstruction on stencil $S_m^{\pm}$, $m = 1, 2, 3$, $p_0^{\pm}(x)$, determined by Eqs. (6) and (7), is the fifth-order reconstruction on stencil $S^{\pm}$. Also,

the set $\{d_0, d_1, d_2, d_3\}$ is the associated linear weights, and the set $\{w_0^\pm, w_1^\pm, w_2^\pm, w_3^\pm\}$ is the associated non-linear weights. The WENO reconstruction (17) is a non-linear convex combination of the polynomials $p_m^\pm(x)$, $m = 0, 1, 2, 3$, thus their ideal weights can be any positive constants with only condition that their sum equals to one. In this paper, the ideal weights are a symmetrical choice, therefore the reconstruction (17) is named as symmetrical WENO reconstruction. The smoothness indicators $\beta_m^\pm$, $m = 0, 1, 2, 3$ are calculated to measure the smoothness of $p_m^\pm(x), m = 0, 1, 2, 3$ on cells I_{x_j} and $I_{x_{j+1}}$, respectively, and are computed by applying various order derivatives. The smaller $\beta_m^\pm$, $m = 0, 1, 2, 3$, the smoother $p_m^\pm(x)$, $m = 0, 1, 2, 3$ are in different target cells. The smoothness indicators are computed as follows [48]

$$\beta_i^- = \sum_{k=1}^r \Delta x^{2k-1} \int_{I_{x_j}} \left(\frac{d^k p_i^-(x)}{dx^k}\right)^2 dx, \quad i = 0, 1, 2, 3, \tag{18}$$

and

$$\beta_i^+ = \sum_{k=1}^r \Delta x^{2k-1} \int_{I_{x_{j+1}}} \left(\frac{d^k p_i^+(x)}{dx^k}\right)^2 dx, \quad i = 0, 1, 2, 3. \tag{19}$$

For $i = 0$, r equals four and if $i = 1, 2, 3$, requals two. Note that, the smoothness indicators can be written as the sum of square terms explicitly

$$\begin{aligned}
\beta_0^- &= \frac{13}{3}\left(-\frac{11}{260}\Delta^-\phi_{j-2} + \frac{87}{130}\Delta^-\phi_{j-1} - \frac{163}{130}\Delta^-\phi_j + \frac{87}{130}\Delta^-\phi_{j+1} - \frac{11}{260}\Delta^-\phi_{j+2}\right)^2 \\
&+ \left(\frac{1}{12}\Delta^-\phi_{j-2} - \frac{2}{3}\Delta^-\phi_{j-1} + \frac{2}{3}\Delta^-\phi_{j+1} - \frac{1}{12}\Delta^-\phi_{j+2}\right)^2 \\
&+ \frac{1421461}{2275}\left(\frac{1}{24}\Delta^-\phi_{j-2} - \frac{1}{6}\Delta^-\phi_{j-1} + \frac{1}{4}\Delta^-\phi_j - \frac{1}{6}\Delta^-\phi_{j+1} + \frac{1}{24}\Delta^-\phi_{j+2}\right)^2 \\
&+ \frac{781}{20}\left(-\frac{1}{12}\Delta^-\phi_{j-2} + \frac{1}{6}\Delta^-\phi_{j-1} - \frac{1}{6}\Delta^-\phi_{j+1} + \frac{1}{12}\Delta^-\phi_{j+2}\right)^2, \\
\beta_1^- &= \frac{13}{3}\left(\frac{1}{2}\Delta^-\phi_{j-2} - \Delta^-\phi_{j-1} + \frac{1}{2}\Delta^-\phi_j\right)^2 + \left(\frac{1}{2}\Delta^-\phi_{j-2} - 2\Delta^-\phi_{j-1} + \frac{3}{2}\Delta^-\phi_j\right)^2, \\
\beta_2^- &= \frac{13}{3}\left(\frac{1}{2}\Delta^-\phi_{j-1} - \Delta^-\phi_j + \frac{1}{2}\Delta^-\phi_{j+1}\right)^2 + \left(-\frac{1}{2}\Delta^-\phi_{j-1} + \frac{1}{2}\Delta^-\phi_{j+1}\right)^2, \\
\beta_3^- &= \frac{13}{3}\left(\frac{1}{2}\Delta^-\phi_j - \Delta^-\phi_{j+1} + \frac{1}{2}\Delta^-\phi_{j+2}\right)^2 + \left(-\frac{3}{2}\Delta^-\phi_j + 2\Delta^-\phi_{j+1} - \frac{1}{2}\Delta^-\phi_{j+2}\right)^2, \\
\beta_0^+ &= \frac{13}{3}\left(-\frac{11}{260}\Delta^-\phi_{j-1} + \frac{87}{130}\Delta^-\phi_j - \frac{163}{130}\Delta^-\phi_{j+1} + \frac{87}{130}\Delta^-\phi_{j+2} - \frac{11}{260}\Delta^-\phi_{j+3}\right)^2 \\
&+ \left(\frac{1}{12}\Delta^-\phi_{j-1} - \frac{2}{3}\Delta^-\phi_j + \frac{2}{3}\Delta^-\phi_{j+2} - \frac{1}{12}\Delta^-\phi_{j+3}\right)^2 \\
&+ \frac{1421461}{2275}\left(\frac{1}{24}\Delta^-\phi_{j-1} - \frac{1}{6}\Delta^-\phi_j + \frac{1}{4}\Delta^-\phi_{j+1} - \frac{1}{6}\Delta^-\phi_{j+2} + \frac{1}{24}\Delta^-\phi_{j+3}\right)^2 \\
&+ \frac{781}{20}\left(-\frac{1}{12}\Delta^-\phi_{j-1} + \frac{1}{6}\Delta^-\phi_j - \frac{1}{6}\Delta^-\phi_{j+2} + \frac{1}{12}\Delta^-\phi_{j+3}\right)^2, \\
\beta_1^+ &= \frac{13}{3}\left(\frac{1}{2}\Delta^-\phi_{j-1} - \Delta^-\phi_j + \frac{1}{2}\Delta^-\phi_{j+1}\right)^2 + \left(\frac{1}{2}\Delta^-\phi_{j-1} - 2\Delta^-\phi_j + \frac{3}{2}\Delta^-\phi_{j+1}\right)^2, \\
\beta_2^+ &= \frac{13}{3}\left(\frac{1}{2}\Delta^-\phi_j - \Delta^-\phi_{j+1} + \frac{1}{2}\Delta^-\phi_{j+2}\right)^2 + \left(-\frac{1}{2}\Delta^-\phi_j + \frac{1}{2}\Delta^-\phi_{j+2}\right)^2, \\
\beta_3^+ &= \frac{13}{3}\left(\frac{1}{2}\Delta^-\phi_{j+1} - \Delta^-\phi_{j+2} + \frac{1}{2}\Delta^-\phi_{j+3}\right)^2 + \left(-\frac{3}{2}\Delta^-\phi_{j+1} + 2\Delta^-\phi_{j+2} - \frac{1}{2}\Delta^-\phi_{j+3}\right)^2.
\end{aligned} \tag{20}$$

As can be seen from Eq. (20), the computation of smooth indicator is a heavy section in the total computation of WENO reconstruction (17). The computational cost of $\beta_0^\pm$ is comparable to the sum of the other three $\beta_m^\pm$, $m = 0, 1, 2$, hence is too heavy. If there exists a discontinuity crossing the stencil of the discretization scheme, the smoothness $\beta_0^\pm$ will always detect it, whatever the location of this discontinuity. Initially, $\beta_0^\pm$ is associated with $p_0^\pm(x)$ of which the role is to help to recover the optimum polynomial $p_0^\pm(x)$ when the solution is smooth on the discretization stencil. On the contrary, when the solution becomes discontinuous, $p_0^\pm(x)$ must always be discarded and the procedure must select between the polynomials $p_1^\pm(x), p_2^\pm(x)$ or $p_3^\pm(x)$. This is the main reason why the definition of $\beta_0^\pm$ is somewhat different from that of $\beta_m^\pm$, $m = 1, 2, 3$. From Taylor series expansions at x_j, we have

$$
\begin{aligned}
\beta_0^- &= \phi_j''^2 \Delta x^2 - \phi_j'' \phi_j''' \Delta x^3 + (\frac{1}{3}\phi_j^{(4)}\phi_j'' + \frac{4}{3}\phi_j'''^2)\Delta x^4 + (-\frac{5}{4}\phi_j^{(4)}\phi_j''' - \frac{1}{12}\phi_j^{(5)}\phi_j'')\Delta x^5 + \mathcal{O}(\Delta x^6), \\
\beta_1^- &= \phi_j''^2 \Delta x^2 - \phi_j'' \phi_j''' \Delta x^3 + (-\frac{1}{3}\phi_j^{(4)}\phi_j'' + \frac{4}{3}\phi_j'''^2)\Delta x^4 + (-\frac{37}{12}\phi_j^{(4)}\phi_j''' + \frac{3}{4}\phi_j^{(5)}\phi_j'')\Delta x^5 + \mathcal{O}(\Delta x^6), \\
\beta_2^- &= \phi_j''^2 \Delta x^2 - \phi_j'' \phi_j''' \Delta x^3 + (\frac{2}{3}\phi_j^{(4)}\phi_j'' + \frac{4}{3}\phi_j'''^2)\Delta x^4 + (-\frac{17}{12}\phi_j^{(4)}\phi_j''' - \frac{1}{4}\phi_j^{(5)}\phi_j'')\Delta x^5 + \mathcal{O}(\Delta x^6), \\
\beta_3^- &= \phi_j''^2 \Delta x^2 - \phi_j'' \phi_j''' \Delta x^3 + (-\frac{1}{3}\phi_j^{(4)}\phi_j'' + \frac{4}{3}\phi_j'''^2)\Delta x^4 + (\frac{5}{4}\phi_j^{(4)}\phi_j''' - \frac{1}{4}\phi_j^{(5)}\phi_j'')\Delta x^5 + \mathcal{O}(\Delta x^6), \\
\beta_0^+ &= \phi_j''^2 \Delta x^2 + \phi_j'' \phi_j''' \Delta x^3 + (\frac{1}{3}\phi_j^{(4)}\phi_j'' + \frac{4}{3}\phi_j'''^2)\Delta x^4 + (\frac{5}{4}\phi_j^{(4)}\phi_j''' + \frac{1}{12}\phi_j^{(5)}\phi_j'')\Delta x^5 + \mathcal{O}(\Delta x^6), \\
\beta_1^+ &= \phi_j''^2 \Delta x^2 + \phi_j'' \phi_j''' \Delta x^3 + (-\frac{1}{3}\phi_j^{(4)}\phi_j'' + \frac{4}{3}\phi_j'''^2)\Delta x^4 + (-\frac{5}{4}\phi_j^{(4)}\phi_j''' + \frac{1}{4}\phi_j^{(5)}\phi_j'')\Delta x^5 + \mathcal{O}(\Delta x^6), \\
\beta_2^+ &= \phi_j''^2 \Delta x^2 + \phi_j'' \phi_j''' \Delta x^3 + (\frac{2}{3}\phi_j^{(4)}\phi_j'' + \frac{4}{3}\phi_j'''^2)\Delta x^4 + (\frac{17}{12}\phi_j^{(4)}\phi_j''' + \frac{1}{4}\phi_j^{(5)}\phi_j'')\Delta x^5 + \mathcal{O}(\Delta x^6), \\
\beta_3^+ &= \phi_j''^2 \Delta x^2 + \phi_j'' \phi_j''' \Delta x^3 + (-\frac{1}{3}\phi_j^{(4)}\phi_j'' + \frac{4}{3}\phi_j'''^2)\Delta x^4 + (\frac{37}{12}\phi_j^{(4)}\phi_j''' - \frac{3}{4}\phi_j^{(5)}\phi_j'')\Delta x^5 + \mathcal{O}(\Delta x^6).
\end{aligned}
\tag{21}
$$

As can be seen from Eq. (21), all the $\beta_m^\pm$, $m = 0, 1, 2, 3$ have the same leading term, therefore have the comparable values in smooth area. For this reason, practically, the definition of $\beta_0^\pm$ may be simplified by using $\max(\beta_1^\pm, \beta_2^\pm, \beta_3^\pm)$ instead.

In order to complete the reconstruction of (17), we calculate the non-linear weights based on the associated linear weights and the smoothness indicators to obtain the fifth-order accuracy for smooth areas and non-oscillatory performance near singularities and discontinuities. Accordingly, we consider

$$
w_i^\pm = \frac{\alpha_i^\pm}{\sum_{k=0}^3 \alpha_k^\pm}, \quad \alpha_i^\pm = d_i\left(1 + \frac{\tau^\pm}{\Delta x^2 + \beta_i^\pm}\right), \quad i = 0, 1, 2, 3,
\tag{22}
$$

where $\tau^\pm$ is simply calculated as

$$
\tau^\pm = |\beta_1^\pm - \beta_3^\pm|.
\tag{23}
$$

Now, we have a new WENO reconstruction for solving HJ equations which its order of accuracy will be discussed in the following. From Taylor series expansions for the polynomials $p_0^\pm(x), p_1^\pm(x), p_2^\pm(x)$ and

$p_3^{\pm}(x)$ at x_j, it can be observed

$$p_0^{\pm}(x_j) = u(x_j) \pm \frac{1}{60}u^{(5)}(x_j)\Delta x^5 + \mathcal{O}(\Delta x^6),$$

$$p_1^-(x_j) = u(x_j) - \frac{1}{4}u'''(x_j)\Delta x^3 + \mathcal{O}(\Delta x^4),$$

$$p_2^-(x_j) = p_1^+(x_j) = u(x_j) + \frac{1}{12}u'''(x_j)\Delta x^3 + \mathcal{O}(\Delta x^4), \tag{24}$$

$$p_3^-(x_j) = p_2^+(x_j) = u(x_j) - \frac{1}{12}u'''(x_j)\Delta x^3 + \mathcal{O}(\Delta x^4),$$

$$p_3^+(x_j) = u(x_j) + \frac{1}{4}u'''(x_j)\Delta x^3 + \mathcal{O}(\Delta x^4),$$

where we apply $u(x_j)$ and $u^{(k)}(x_j)$ to denote $\frac{\partial}{\partial x}\phi(x,t^n)|_{x=x_j}$ and $\frac{\partial^{k+1}}{\partial x^{k+1}}\phi(x,t^n)|_{x=x_j}$, respectively. It should be noted that $p_0^{\pm}(x_j) = \sum_{i=1}^{3}\gamma_i^{\pm}p_i^{\pm}(x_j)$ where $(\gamma_1^-,\gamma_2^-,\gamma_3^-) = (0.1,0.6,0.3)$ and $(\gamma_1^+,\gamma_2^+,\gamma_3^+) = (0.3,0.6,0.1)$. By using Eq. (24), the WENO reconstruction (17) can be written as follows:

$$\begin{aligned}
u_j^{\pm} :=\ & \frac{w_0^{\pm}}{d_0}\left[\sum_{i=1}^{3}\gamma_i^{\pm}p_i^{\pm}(x_j) - d_1 p_1^{\pm}(x_j) - d_2 p_2^{\pm}(x_j) - d_3 p_3^{\pm}(x_j)\right] \\
& + w_1^{\pm}p_1^{\pm}(x_j) + w_2^{\pm}p_2^{\pm}(x_j) + w_3^{\pm}p_3^{\pm}(x_j) \\
=\ & \sum_{i=1}^{3}\left(\frac{\gamma_i^{\pm} - d_i}{d_0}w_0^{\pm} + w_i^{\pm}\right)p_i^{\pm}(x_j) \\
=\ & \sum_{i=1}^{3}\gamma_i^{\pm}p_i^{\pm}(x_j) + \sum_{i=1}^{3}\left(\frac{\gamma_i^{\pm} - d_i}{d_0}w_0^{\pm} + w_i^{\pm} - \gamma_i^{\pm}\right)p_i^{\pm}(x_j) \\
=\ & \left(u(x_j) + \mathcal{O}(\Delta x^5)\right) + \sum_{i=1}^{3}\left(\frac{\gamma_i^{\pm} - d_i}{d_0}w_0^{\pm} + w_i^{\pm} - \gamma_i^{\pm}\right)u(x_j) \\
& + \sum_{i=1}^{3}\left(\frac{\gamma_i^{\pm} - d_i}{d_0}w_0^{\pm} + w_i^{\pm} - \gamma_i^{\pm}\right)A_j^{\pm}\Delta x^3 \\
& + \sum_{i=1}^{3}\left(\frac{\gamma_i^{\pm} - d_i}{d_0}w_0^{\pm} + w_i^{\pm} - \gamma_i^{\pm}\right)\mathcal{O}(\Delta x^4),
\end{aligned} \tag{25}$$

where $\left(A_1^-, A_2^- = A_1^+, A_3^- = A_2^+, A_3^+\right) = \left(-\frac{3}{12}, \frac{1}{12}, -\frac{1}{12}, \frac{3}{12}\right)u'''(x_j)$.

Since $\sum_{i=1}^{3}\gamma_i^{\pm} = \sum_{i=0}^{3}d_i = \sum_{i=0}^{3}w_i^{\pm} = 1$, one can easily obtain

$$\sum_{i=1}^{3}\left(\frac{\gamma_i^{\pm} - d_i}{d_0}w_0^{\pm} + w_i^{\pm} - \gamma_i^{\pm}\right) = 0, \tag{26}$$

accordingly, in order to have the fifth-order of accuracy, we only need to have

$$\sum_{i=1}^{3}\left(\frac{\gamma_i^{\pm} - d_i}{d_0}w_0^{\pm} + w_i^{\pm} - \gamma_i^{\pm}\right)A_j^{\pm} \leq \mathcal{O}(\Delta x^2), \tag{27}$$

or

$$\begin{cases} w_0^\pm - d_0 \leq \mathcal{O}(\Delta x^2), \\[2mm] (3d_1 - d_2 + d_3)w_0^- - 3d_0 w_1^- + d_0 w_2^- - d_0 w_3^- \leq \mathcal{O}(\Delta x^2), \\[2mm] (-d_1 + d_2 - 3d_3)w_0^+ + d_0 w_1^+ - d_0 w_2^+ + 3d_0 w_3^+ \leq \mathcal{O}(\Delta x^2). \end{cases} \tag{28}$$

Using Eqs. (21) and (23), the truncation error of $\tau^\pm$ is

$$\tau^\pm = |\frac{13}{3}\phi_j^{(4)}\phi_j''' - \phi_j^{(5)}\phi_j''|\Delta x^5 + \mathcal{O}(\Delta x^6). \tag{29}$$

Thus, it can be seen that

$$\left(1 + \frac{\tau^\pm}{\Delta x^2 + \beta_i^\pm}\right) = 1 + \mathcal{O}(\Delta x^3), \quad i = 0, 1, 2, 3. \tag{30}$$

It is essential to point out that Eq. (30) hold even at the critical points where the first and the higher derivatives are zero. Because of the Taylor expansion

$$\frac{1}{1+x} = 1 - x + x^2 - \cdots,$$

and from Eq. (22), it is easy to derive

$$w_i^\pm = d_i + \mathcal{O}(\Delta x^3), \quad i = 0, 1, 2, 3. \tag{31}$$

Hence

$$\begin{aligned} (3d_1 - d_2 + d_3)w_0^- - 3d_0 w_1^- + d_0 w_2^- - d_0 w_3^- = \\ (3d_1 - d_2 + d_3)d_0 - 3d_0 d_1 + d_0 d_2 - d_0 d_3 + \mathcal{O}(\Delta x^3) = 0 + \mathcal{O}(\Delta x^3), \\ (-d_1 + d_2 - 3d_3)w_0^+ + d_0 w_1^+ - d_0 w_2^+ + 3d_0 w_3^+ = \\ (-d_1 + d_2 - 3d_3)d_0 + d_0 d_1 - d_0 d_2 + 3d_0 d_3 + \mathcal{O}(\Delta x^3) = 0 + \mathcal{O}(\Delta x^3), \end{aligned} \tag{32}$$

therefore, the condition (28) is satisfied and the designed fifth-order accuracy for the new reconstruction is obtained even near the critical points where the first and higher derivatives zero.

3 Computational results

In this section, the numerical results of the proposed scheme, named as SWENO-A, will be reviewed and compared with WENO-ZQ [48] and WENO-JP [22] schemes. It should be noted that SWENO-A uses the fifth-order five-step high-order linear multi-step scheme, $\text{TVB}_0(5,5)$ [35], to progress in time. The constant CFL number $c = 0.3$ is considered. The "dimension-by-dimension" technique is used to extend

the described scheme to solve the multi-dimensional problems. Let $u(x_j, t^n)$ and w_j^n be the exact solution and the reconstructed solution respectively at (x_j, t^n). Then the norms of the error are given by:

$$L_1 - \text{error}: \quad ||u - w||_1 = \sum_{j=1}^{N} |u(x_j, t^n) - w_j^n| \Delta x,$$

$$L_\infty - \text{error}: \quad ||u - w||_\infty = \max_{1 \leqslant j \leqslant N} |u(x_j, t^n) - w_j^n|.$$

Example 1. As the first example, we examine the accuracy and order of convergence of schemes by the Burgers' equation in two and three dimensional space. First, consider the following non-linear scalar 2D Burgers equation:

$$\phi_t + \frac{1}{2}(\phi_x + \phi_y + 1)^2 = 0, \quad -2 \leq x, y \leq 2, \tag{33}$$

with the initial condition $\phi(x, y, 0) = -\cos(\pi(x + y)/2)$ and periodic boundary conditions. The solution is still smooth at $T = 0.5/\pi^2$. The results are computed at that time and the errors and orders of accuracy by methods are shown in Table 1. It can be observed that the order is achieved and the SWENO-A scheme can get better results and is more efficient than WENO-JP and WENO-ZQ. Now, consider the following non-linear scalar 3D Burgers' equation

$$\phi_t + \frac{1}{2}(\phi_x + \phi_y + \phi_z + 1)^2 = 0, \quad -3 \leq x, y, z \leq 3, \tag{34}$$

with the initial condition $\phi(x, y, z, 0) = -\cos(\pi(x + y + z)/3)$ and periodic boundary conditions. The results are computed at $T = 0.5/\pi^2$ and the errors and orders of accuracy by all schemes are demonstrated in Table 2. We can see that the order is achieved and the SWENO-A scheme can get better results and is more efficient than WENO-JP and WENO-ZQ.

Example 2. Now to investigate the behavior of the proposed scheme close to the steep gradients, the linear equation $\phi_t + \phi_x = 0$ with the following initial condition is considered

$$\phi(x, 0) = \begin{cases} \frac{1}{6}(G(x, z - \delta) + G(x, z + \delta) + 4G(x, z)), & -0.6 \leq x \leq -0.4, \\ 1 - 10|x|, & -0.1 \leq x \leq 0.1, \\ \frac{1}{6}(F(x, a - \delta) + F(x, a + \delta) + 4F(x, a)), & 0.4 \leq x \leq 0.6, \\ 0, & \text{otherwise}, \end{cases} \tag{35}$$

where $G(x, z) = e^{-\beta(x-z)^2}$ and $F(x, a) = (\max(1 - \alpha^2(x - a)^2, 0))^{1/2}$. The constants in these functions are: $a = 0.5$, $z = -0.5$, $\delta = 0.005$, $\alpha = 10$ and $\beta = (\log 2)/36\delta^2$. In this problem, the periodic boundary conditions are assigned. Eq. (35) contains a Gaussian, a sharp triangle wave, and a half ellipse. The numerical results obtained at the final time $T = 10$, in which the computational domain $[-1, 1]$ is divided into $N = 150$ sub-equal intervals, are shown in Fig. 1. As can be seen, all numerical schemes have produced almost non-oscillatory solutions and the Gibbs oscillations are not significant, but in general the SWENO-A scheme has better results for all types of waves than the other schemes.

Example 3. Now in this example, the 1D non-linear Burgers' equation

$$\phi_t + \frac{1}{2}(\phi_x + 1)^2 = 0, \quad -1 \leq x \leq 1, \tag{36}$$

Table 1: L_1 and L_∞ errors and the order of convergence for Eq. (33). $(A(-e) := A \times 10^{-e})$

	WENO-JP				WENO-ZQ			
N	L_1-error	L_1-order	L_∞-error	L_∞-order	L_1-error	L_1-order	L_∞-error	L_∞-order
10	2.83(-02)	-	4.70(-02)	-	1.57(-02)	-	2.03(-02)	-
20	1.20(-03)	4.56	2.40(-03)	4.29	5.42(-04)	4.86	1.31(-03)	3.95
40	4.13(-05)	4.86	7.20(-05)	5.06	8.75(-06)	5.95	1.59(-05)	6.36
80	1.47(-06)	4.81	2.30(-06)	4.97	2.21(-07)	5.31	3.41(-07)	5.54
160	4.42(-08)	5.06	7.01(-08)	5.04	6.66(-09)	5.05	1.14(-08)	4.90
320	1.46(-09)	4.92	2.27(-09)	4.95	2.13(-10)	4.97	3.31(-10)	5.11

	SWENO-A			
N	L_1-error	L_1-order	L_∞-error	L_∞-order
10	2.19(-03)	-	2.77(-03)	-
20	5.94(-05)	5.20	2.05(-04)	3.76
40	9.26(-07)	6.00	2.41(-06)	6.41
80	2.91(-08)	4.99	4.11(-08)	5.87
160	7.36(-10)	5.31	1.89(-09)	4.50
320	2.53(-11)	4.86	4.14(-11)	5.46

Table 2: L_1 and L_∞ errors and the order of convergence for Eq. (34). $(A(-e) := A \times 10^{-e})$

	WENO-JP				WENO-ZQ			
N	L_1-error	L_1-order	L_∞-error	L_∞-order	L_1-error	L_1-order	L_∞-error	L_∞-order
20	2.83(-04)	-	1.85(-03)	-	1.56(-04)	-	6.35(-04)	-
40	1.41(-05)	4.33	1.67(-04)	3.47	6.03(-06)	4.69	6.69(-05)	3.25
80	5.39(-07)	4.71	6.68(-06)	4.64	2.31(-07)	4.71	2.90(-06)	4.53
160	2.02(-08)	4.74	2.36(-07)	4.82	7.49(-09)	4.95	9.83(-08)	4.88
320	6.72(-10)	4.91	7.23(-09)	5.03	2.44(-10)	4.94	3.23(-09)	4.93

	SWENO-A			
N	L_1-error	L_1-order	L_∞-error	L_∞-order
20	2.24(-05)	-	7.01(-05)	-
40	6.72(-07)	5.06	7.48(-06)	3.23
80	3.16(-08)	4.41	3.63(-07)	4.36
160	8.25(-10)	5.26	1.52(-08)	4.58
320	3.09(-11)	4.74	3.88(-10)	5.29

with the initial condition $\phi(x,0) = -\cos(\pi x)$ and the periodic boundary conditions is solved. The solution to this equation has discontinuous derivative when $T = 1.5/\pi^2$, so the results of the schemes at this time are shown in Fig. 2. From this figure it can be concluded that the results of the schemes are comparable and SWENO-A has produced good results for this test case.

Example 4. Now consider, the 2D non-linear HJ equations

$$\phi_t + H(\phi_x, \phi_y) = 0, \quad -2 \leq x, y \leq 2, \tag{37}$$

with the initial condition $\phi(x,y,0) = -\cos(\pi(x+y)/2)$ and periodic boundary conditions. In this example, two types of Hamiltonian are considered, one convex $H(u,v) = \frac{1}{2}(u+v+1)^2$ and the other non-convex $H(u,v) = -\cos(u+v+1)$. It should be noted that the singularity occurs at time $T = 1/\pi^2$
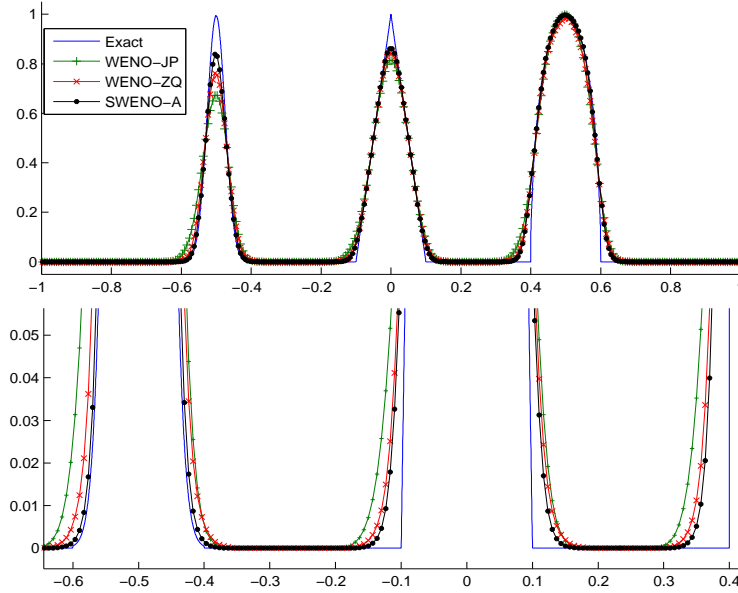
Figure 1: Top: Example 2 at the finial time $T = 10$ and $N = 150$. Bottom: Zoomed region.

for the convex Hamiltonian and near this time for the non-convex case. The results of SWENO-A for the two types of Hamiltonian after the formation of singularity at time $T = 1.5/\pi^2$ are shown in Fig. 3 and can be seen to provide good results.

Example 5. In this example, a 2D non-convex Riemann problem [31]

$$\phi_t + \sin(\phi_x + \phi_y) = 0, \quad -1 \leq x, y \leq 1, \tag{38}$$

with the initial condition $\phi(x, y, 0) = \pi(|y| - |x|)$ and fixed boundary conditions is solved. The results are compute up to $T = 1$ with $N_x \times N_y = 40 \times 40$. We present the numerical resolution of SWENO-A in Fig. 4 and the results compare well with those reported in [48].

Example 6. In this example, we solve a 2D non-convex problem, known as Eikonal equation,

$$\phi_t + \sqrt{\phi_x^2 + \phi_y^2 + 1} = 0, \quad 0 \leq x, y \leq 1, \tag{39}$$

with initial condition $\phi(x, y, 0) = \frac{1}{4}(\cos(2\pi x) - 1)(\cos(2\pi y) - 1) - 1$ and periodic boundary conditions. This problem arises in geometric optics [24]. The data after singularity at $T = 0.6$ is recorded with $N_x \times N_y = 40 \times 40$ and the numerical solution of SWENO-A is presented in Fig. 5. The results compare well with those reported in [48].

Example 7. In this example, a problem from optimal control

$$\phi_t - (\sin y)\phi_x + (\sin x + sign(\phi_y))\phi_y - \frac{1}{2}\sin^2 y - (1 - \cos x) = 0, \quad -\pi \leq x, y \leq \pi, \tag{40}$$
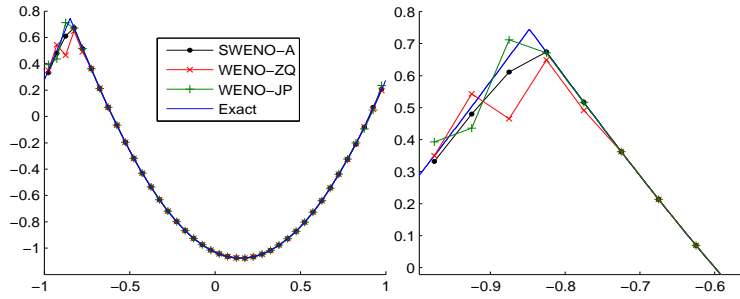
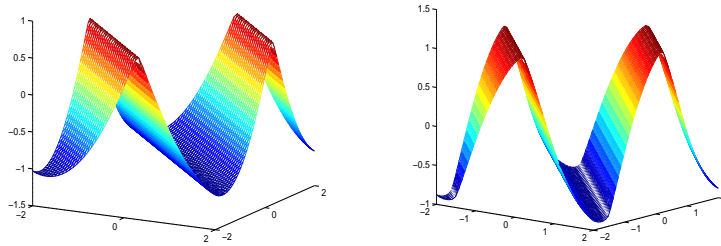Figure 2: Example 3 by $N = 40$. Left: Burgers' equation. Right: Zoomed regions.

Figure 3: Example 4 by $N_x \times N_y = 40 \times 40$. Left: Convex Hamiltonian. Right: Non-convex Hamiltonian.

with initial condition $\phi(x,y,0) = 0$ and periodic boundary conditions is considered. Numerical results by the new proposed scheme at $T = 1$ with $N_x \times N_y = 40 \times 40$ is plotted in Fig. 6 and the results compare well with those reported in [48].

Example 8. Finally, the problem of a propagating surface, introduced in [30],

$$\phi_t - (1 - \varepsilon K)\sqrt{\phi_x^2 + \phi_y^2 + 1} = 0, \quad 0 \le x, y \le 1, \tag{41}$$

with initial condition $\phi(x,y,0) = 1 - \frac{1}{4}(\cos(2\pi x) - 1)(\cos(2\pi y) - 1)$ and periodic boundary conditions is considered. Here ε is a small constant and K is the mean curvature defined by

$$K = -\frac{\phi_{xx}(1 + \phi_y^2) - 2\phi_{xy}\phi_x\phi_y + \phi_{yy}(1 + \phi_x^2)}{(1 + \phi_x^2 + \phi_y^2)^{\frac{3}{2}}},$$

that it is computed by using central differences. The numerical results generated by SWENO-A are plotted in Fig. 7. It should be noted that the solution at $T = 0.1$ for $\varepsilon = 0.1$ is shifted downward in order to show the details of the solution at later time. The results compare well with those reported in [48].

Now to compare the schemes from CPU times perspective, Table 3 shows the CPU times of each schemes for a number of examples. Since SWENO-A has an additional reconstruction compared to
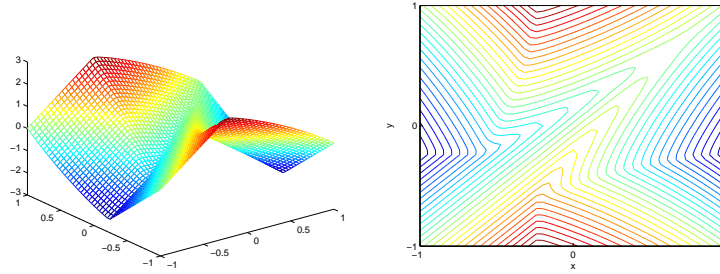
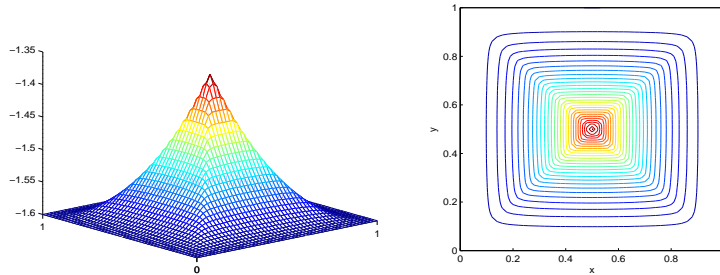Figure 4: Example 5 by $N_x \times N_y = 40 \times 40$ at $T = 1$.

Figure 5: Example 6 by $N_x \times N_y = 40 \times 40$ at $T = 0.6$.

WENO-ZQ and WENO-JP, the speed-up ("speed-up" is obtained as the ratio of the CPU time of SWENO-A to that of WENO-JP and WENO-ZQ) of SWENO-A is greater than 1, which means that SWENO-A reconstruction is more expensive than WENO-ZQ and WENO-JP reconstructions, but the speed-up is always close to 1. This means that extra work is minor compared to the necessary WENO reconstruction steps. Therefore, the extra computational time of SWENO-A is not significant to obtain higher accuracy and resolution. Finally, a numerical stability study, checking the stability properties of 3D schemes, is presented. The relative L_1 errors for Example 1 (Eq. (34)) while varying the CFL number are shown in Fig. 8. The stability properties of SWENO-A are similar to the stability properties of WENO-ZQ and WENO-JP, but SWENO-A enjoys smaller L_1 errors and hence is more accurate after the formation of the singularity. Since non-smooth cases are expected for WENO schemes, we prefer to employ SWENO-A for solving HJ equations after the singularity formation.

4   Conclusion

In this paper, a new symmetrical WENO interpolation procedure for 1D HJ equations is constructed. Afterwards, this procedure is straightforwardly extended to multi-dimensional HJ equations. This interpolation results from a convex combination of various polynomials. Combined with $TVB_0(5, 5)$ method for advancing in time, this procedure produces a fifth-order scheme in smooth areas and maintains non-oscillatory properties for problems with strong discontinuous derivative. In comparison with WENO-
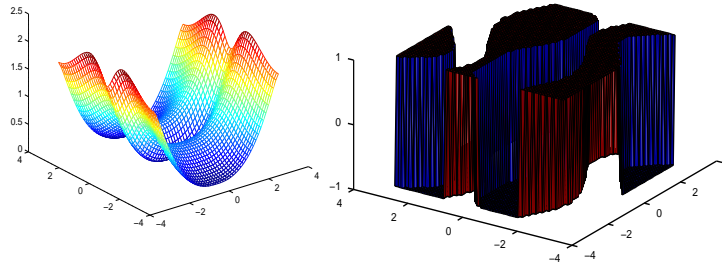
Figure 6: Example 7 by $N_x \times N_y = 40 \times 40$ at $T = 1$. Left: surfaces of the solution. Right: the optimal control $\omega = sign(\phi_y)$.

Table 3: Computational times in seconds for some examples presented in this work. Top to Bottom: Example 1 Eq. (33), Example 1 Eq. (34) and Example 8 at $T = 0.6$ with $\varepsilon = 0.1$

Number of cells	WENO-JP	WENO-ZQ	SWENO-A	ratio=$\frac{SWENO-A}{WENO-JP}$	ratio=$\frac{SWENO-A}{WENO-ZQ}$
320×320	4.117	3.993	4.216	1.024047	1.055848
$320 \times 320 \times 320$	27.381	26.261	27.891	1.018626	1.062069
40×40	46.391	44.763	48.003	1.034748	1.072381

JP [22] and WENO-ZQ [48] schemes for solving HJ equations, it was observed that SWENO-A scheme gives better resolution than WENO-JP and WENO-ZQ schemes and has smaller errors after the singularity formation. Similar to WENO-JP and WENO-ZQ schemes, the order of accuracy of SWENO-A scheme has been reduced after the formation of the singularity.

Acknowledgements

References

[1] R. Abedian, *High-order semi-discrete central-upwind schemes with Lax-Wendroff-Type time discretizations for Hamilton-Jacobi equations*, Comput. Methods Appl. Math. **18** (2018) 559–580.

[2] R. Abedian, *A symmetrical WENO-Z scheme for solving Hamilton-Jacobi equations*, Int. J. Mod. Phys. C **31** (2020) 2050039.

[3] R. Abedian, H. Adibi, M. Dehghan, *Symmetrical weighted essentially non-oscillatory-flux limiter schemes for Hamilton-Jacobi equations*, Math. Methods Appl. Sci. **38** (2015) 4710–4728.
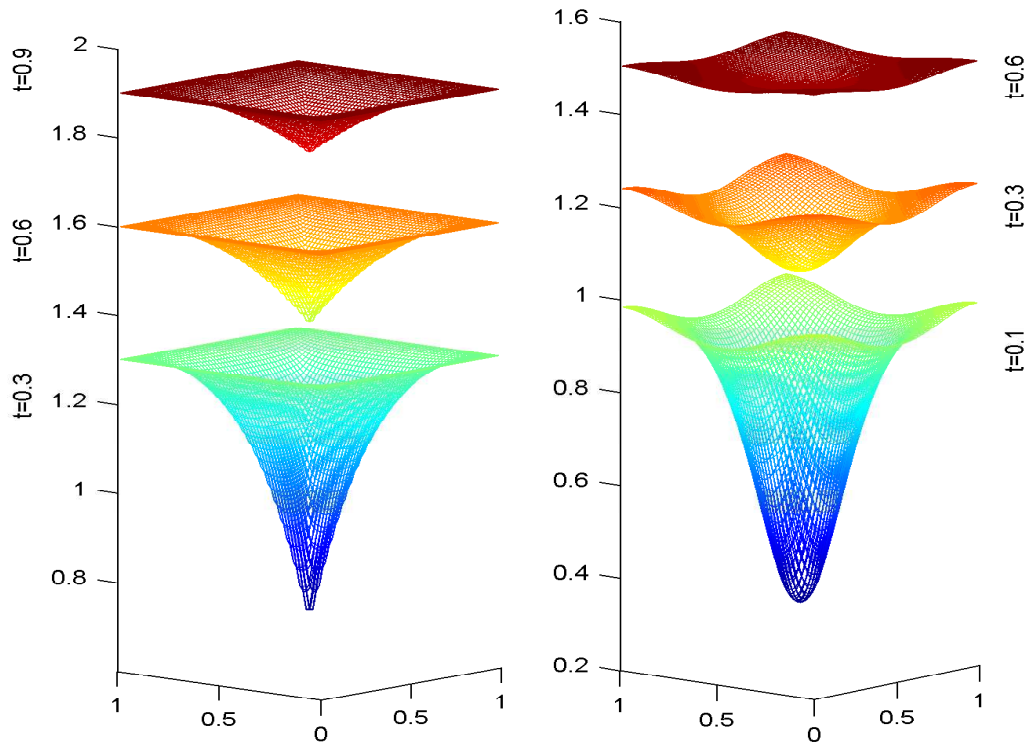
Figure 7: Example 8 by $N_x \times N_y = 40 \times 40$. Left: $\varepsilon = 0$. Right: $\varepsilon = 0.1$.

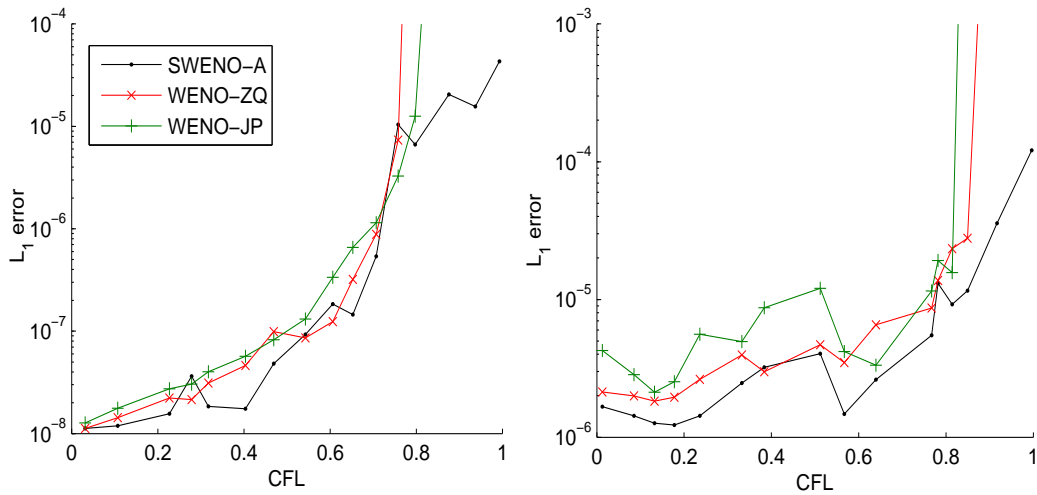
Figure 8: Stability of the 3D SWENO-A, WENO-ZQ and WENO-JP with $N_x \times N_y \times N_z = 80 \times 80 \times 80$. The L_1 errors are plotted against the different CFL number. Left: Eq.(34) before the singularity at $T = 0.5/\pi^2$. Right: Eq. (34) after the singularity at $T = 1.5/\pi^2$.

[4] R. Abedian, M. Dehghan, *RBF-ENO/WENO schemes with Lax-Wendroff type time discretizations for Hamilton-Jacobi equations*, Numer. Methods Partial Differential Equations **37** (2021) 594–613.

[5] R. Abedian, R. Salehi, *A RBFWENO finite difference scheme for Hamilton-Jacobi equations*, Comput. Math. Appl. **79** (2020) 2002–2020.

[6] R. Abgrall, *Numerical discretization of the first-order Hamilton-Jacobi equation on triangular meshes*, Comm. Pure Appl. Math. **49** (1996) 1339–1373.

[7] D. S. Balsara, S. K. Garain, C.-W. Shu, *An efficient class of WENO schemes with adaptive order*, J. Comput. Phys. **326** (2016) 780–804.

[8] F. Bass, V. Freilikher, A. A. Maradudin, V. Prosentsov, *Geometrical optics approximation for nonlinear equations*, SIAM J. Appl. Math. **64** (2004) 1125–1132.

[9] R. Borges, M. Carmona, B. Costa, W. S. Don, *An improved weighted essentially non-oscillatory scheme for hyperbolic conservation laws*, J. Comput. Phys. **227** (2008) 3191–3211.

[10] S. Bryson, D. Levy, *Mapped WENO and weighted power ENO reconstructions in semi-discrete central schemes for Hamilton-Jacobi equations*, Appl. Numer. Math. **56** (2006) 1211–1224.

[11] R. Buckdahn, J. Li, *Stochastic differential games and viscosity solutions of Hamilton-Jacobi-Bellman-Isaacs equations*, SIAM J. Control Optim. **47** (2008) 444–475.

[12] B. Cockburn, J. Qian, *Continuous dependence results for Hamilton-Jacobi equations*, (2002) 67–90, In D. Estep and S. Tavener Collected Lectures on the Preservation of Stability Under Discretization. SIAM, Philadelphia, PA.

[13] M.G. Crandall, H. Ishii, P.-L. Lions, *User's guide to viscosity solutions of second order partial differential equations*, Bull. Amer. Math. Soc. **27** (1992) 1–67.

[14] M.G. Crandall, P.-L. Lions, *Viscosity solutions of Hamilton-Jacobi equations*, Trans. Amer. Math. Soc. **277** (1983) 1–42.

[15] M.G. Crandall, P.-L. Lions, *Two approximations of solutions of Hamilton-Jacobi equations*, Math. Comput. **43** (1984) 1–19.

[16] S. Gottlieb, C.-W. Shu, *Total variation diminishing Runge-Kutta schemes*, Math. Comp. **67** (1998) 73–85.

[17] S. Gottlieb, C.-W. Shu, E. Tadmor, *Strong stability-preserving high-order time discretization methods*, SIAM Rev. **43** (2001) 89–112.

[18] Y. Ha, C. H. Kim, H. Yang, J. Yoon, *A sixth-order weighted essentially non-oscillatory schemes based on exponential polynomials for Hamilton-Jacobi equations*, J. Sci. Comput. **75** (2018) 1675–1700.

[19] A. Harten, B. Engquist, S. Osher, S. Chakravarthy, *Uniformly high-order essentially non-oscillatory schemes, III*, J. Comput. Phys. **71** (1987) 231–303.

[20] A.K. Henrick, T.D. Aslam, J.M. Powers, *Mapped weighted essentially non-oscillatory schemes: Achieving optimal order near critical points*, J. Comput. Phys. **207** (2005) 542–567.

[21] C. Huang, L.L. Chen, *A simple smoothness indicator for the WENO scheme with adaptive order*, J. Comput. Phys. **352** (2018) 498–515.

[22] G.-S. Jiang, D. Peng, *Weighted ENO schemes for Hamilton-Jacobi equations*, SIAM J. Sci. Comput. **21** (2000) 2126–2143.

[23] G.-S. Jiang, C.-W. Shu, *Efficient implementation of weighted ENO schemes*, J. Comput. Phys. **126** (1996) 202–228.

[24] S. Jin, Z. Xin, *Numerical passage from systems of conservation laws to Hamilton-Jacobi equations and relaxation schemes*, SIAM J. Numer. Anal. **35** (1998) 2163–2186.

[25] F. Lafon, S. Osher, *High order two dimensional nonoscillatory methods for solving Hamilton-Jacobi scalar equations*, J. Comput. Phys. **123** (1996) 235–253.

[26] P.-L. Lions, *Generalized Solutions of Hamilton-Jacobi Equations*, Pitman, London, 1982.

[27] P. L. Lions, *Optimal control of diffusion processes and hamilton-jacobi-bellman equations part2: viscosity solutions and uniqueness*, Commun. Part. Diff. Equ. **8** (1983) 1229–1276.

[28] P.-L. Lions, P. E. Souganidis, *Convergence of MUSCL and filtered schemes for scalar conservation laws and Hamilton-Jacobi equations*, Numer. Math. **69** (1995) 441–470.

[29] X.-D. Liu, S. Osher, T. Chan, *Weighted essentially non-oscillatory schemes*, J. Comput. Phys. **115** (1994) 200–212.

[30] S. Osher, J. Sethian, *Fronts propagating with curvature dependent speed: algorithms based on Hamilton-Jacobi formulations*, J. Comput. Phys. **79** (1988) 12–49.

[31] S. Osher, C.-W. Shu, *High-order essentially nonoscillatory schemes for Hamilton-Jacobi equations*, SIAM J. Numer. Anal. **28** (1991) 907–922.

[32] J. Qiu, *Hermite WENO schemes with Lax-Wendroff type time discretizations for Hamilton-Jacobi equations*, J. Comput. Math. **25** (2007) 131–144.

[33] J. Qiu, *WENO schemes with Lax-Wendroff type time discretizations for Hamilton-Jacobi equations*, J. Comput. Appl. Math. **200** (2007) 591–605.

[34] J. Qiu, C.-W. Shu, *Hermite WENO schemes for Hamilton-Jacobi equations*, J. Comput. Phys. **204** (2005) 82–99.

[35] S.J. Ruuth, W. Hundsdorfer, *High-order linear multistep methods with general monotonicity and boundedness properties*, J. Comput. Phys. **209** (2005) 226–248.

[36] S. Serna, A. Marquina, *Power ENO methods: a fifth-order accurate weighted power ENO method*, J. Comput. Phys. **194** (2004) 632–658.

[37] S. Serna, J. Qian, *Fifth order weighted power-ENO methods for Hamilton-Jacobi equations*, J. Sci. Comput. **29** (2006) 57–81.

[38] C.-W. Shu, *Total-variation-dimishing time discretizations*, SIAM J. Sci. Stat. Comp. **9** (1988) 1073–1084.

[39] C.-W. Shu, S. Osher, *Efficient implementation of essentially non-oscillatory shock-capturing schemes*, J. Comput. Phys. **77** (1988) 439–471.

[40] C.-W. Shu, S. Osher, *Efficient implementation of essentially non-oscillatory shock-capturing schemes II*, J. Comput. Phys. **83** (1989) 32–78.

[41] K. Siddiqi, S. Bouix, A. Tannenbaum, S. W. Zucker, *Hamilton-Jacobi Skeletons*, Int. J. Comput. Vision **48** (2002) 215–231.

[42] P.E. Souganidis, *Approximation schemes for viscosity solutions of Hamilton-Jacobi equations*, J. Differential Equations **59** (1985) 1–43.

[43] Z. Tao, F. Li, J. Qiu, *High-order central Hermite WENO schemes: Dimension-by-dimension moment-based reconstructions*, J. Comput. Phys. **318** (2016) 222–251.

[44] Z. Tao, J. Qiu, *Dimension-by-dimension moment-based central Hermite WENO schemes for directly solving Hamilton-Jacobi equations*, Adv. Comput. Math. **43** (2017) 1023–1058.

[45] Y.-T. Zhang, C.-W. Shu, *High-order WENO schemes for Hamilton-Jacobi equations on triangular meshes*, SIAM J. Sci. Comput. **24** (2003) 1005–1030.

[46] F. Zheng, J. Qiu, *Directly solving the Hamilton-Jacobi equations by Hermite WENO schemes*, J. Comput. Phys. **307** (2016) 423–445.

[47] F. Zheng, C.-W. Shu, J. Qiu, *Finite difference Hermite WENO schemes for the Hamilton-Jacobi equations*, J. Comput. Phys. **337** (2017) 27–41.

[48] J. Zhu, J. Qiu, *A new fifth order finite difference WENO scheme for Hamilton-Jacobi equations*, Numer. Methods Partial Differential Equations **33** (2017) 1095–1113.